Integrative Biology

Cite this: *Integr. Biol.*, 2012, **4**, 401–409

www.rsc.org/ibiology

PAPER

Migration dynamics of breast cancer cells in a tunable 3D interstitial flow chamber†‡

Ulrike Haessler,§[a] Jeremy C. M. Teo,§[a] Didier Foretay,[a] Philippe Renaud[b] and Melody A. Swartz¶*[acd]

Received 5th October 2011, Accepted 17th November 2011
DOI: 10.1039/c1ib00128k

The migration of cells such as leukocytes, tumor cells, and fibroblasts through 3D matrices is critical for regulating homeostasis and immunity and for driving pathogenesis. Interstitial flow through the extracellular matrix, which can substantially increase during inflammation and in the tumor microenvironment, can influence cell migration in multiple ways. Leukocytes and tumor cells are heterogeneous in their migration responses to flow, yet most 3D migration studies use endpoint measurements representing average characteristics. Here we present a robust new microfluidic device for 3D culture with live imaging under well-controlled flow conditions, along with a comparison of analytical methods for describing the migration behavior of heterogeneous cell populations. We then use the model to provide new insight on how interstitial flow affects MDA-MB-231 breast cancer cell invasion, phenomena that are not seen from averaged or endpoint measurements. Specifically, we find that interstitial flow increases the percentage of cells that become migratory, and increases migrational speed in about 20% of the cells. It also increases the migrational persistence of a subpopulation (5–10% of cells) in the positive or negative flow direction. Cells that migrated upstream moved faster but with less directedness, whereas cells that migrated in the direction of flow moved at slower speeds but with higher directedness. These findings demonstrate how fluid flow in the tumor microenvironment can enhance tumor cell invasion by directing a subpopulation of tumor cells in the flow direction; *i.e.*, towards the draining lymphatic vessels, a major route of metastasis.

[a] *Institute of Bioengineering, School of Life Sciences, École Polytechnique Fédérale de Lausanne (EPFL), 1015 Lausanne, Switzerland*
[b] *Institute of Microengineering, School of Engineering, École Polytechnique Fédérale de Lausanne (EPFL), 1015 Lausanne, Switzerland*
[c] *Institute of Chemical Sciences and Engineering, School of Basic Sciences, École Polytechnique Fédérale de Lausanne (EPFL), 1015 Lausanne, Switzerland*
[d] *Swiss Institute for Experimental Cancer Research, École Polytechnique Fédérale de Lausanne (EPFL), 1015 Lausanne, Switzerland*

† Published as part of an iBiology themed issue entitled "From Single Cells to Biology". Editors: Dr Mina Bissell, Distinguished Scientist, and Prof. Luke Lee.

‡ Electronic supplementary information (ESI) available. See DOI: 10.1039/c1ib00128k

§ These authors contributed equally.

¶ SV-IBI-LLCB, Station 15, EPFL, CH-1015 Lausanne, Switzerland. E-mail: melody.swartz@epfl.ch; Fax: +41 (0)21-693-9670; Tel: +41 (0)21-693-9686.

Introduction

The ability of a cell to migrate through a 3D extracellular matrix (ECM) is important for a wide variety of physiological and pathological processes, including development, immune cell surveillance and trafficking, and tumor invasion and metastasis. Cell migration mechanisms may include proteolytic degradation[1–3] or amoeboid-like deformation through pores in the ECM,[4,5] both of which are significantly influenced by ECM properties like its composition and its mechanical stiffness.[6–8] The ECM also provides binding sites for many growth factors and cytokines[9,10] such as VEGF and TGF-β that can be stored in latent forms and locally activated by proteolysis or mechanical stress.[11–13] Thus, experimental models of cell migration critically

Insight, innovation, integration

The migration behavior of cancer cells and leukocytes within 3D matrices under physiological interstitial flow conditions is heterogeneous, with different cell subpopulations responding to different cues that determine their migration path. By using a novel 3D flow chamber culture device that is simple and robust along with comparative analysis methods, we show that interstitial flow increases the overall motility and speed of cancer cells. We further show that minority subpopulations of cells specifically respond to flow in different ways, including flow-directed invasion in roughly 10% of cells. This integration of new technology and analytical approaches to single-cell migration parameters with studies of cancer cell migration allows new insight into the migration dynamics and invasion mechanisms of heterogeneous cancer cell populations.

require specific features of the 3D environment to be recapitulated.

In addition to ECM properties, mechanical forces like interstitial fluid flow[14] can also affect cell migration. Interstitial flow is driven by hydrostatic and osmotic pressure gradients that exist between arterioles, the interstitial space, lymphatic capillaries, and post-capillary venules,[15] and fluid flow between the blood to the lymphatics can be dramatically increased under pathological conditions such as inflammation and cancer.[14,16,17] Interstitial flow has been hypothesized to affect cell migration in a number of different ways, including matrix stiffening and local strain gradient induction,[18–21] flow-upregulated proteolysis by migrating cells,[3,22] stress-mediated cytokine activation,[23] and autologous chemotaxis.[23–25] In the latter mechanism, autologously secreted (or activated) chemokine forms local pericellular diffusion gradients skewed by fluid convection, and the cells subsequently "chemotact" up the flow-directed gradient; this requires that the migrating cell expresses both the chemokine to which it is chemotactically sensitive as well as its receptor, such as CCL19/CCR7 by dendritic cells[26] and some types of invasive tumor cells.[24] In contrast, cells can move upstream of flow in a newly described integrin-mediated mechanism that is CCR7 independent.[20] The net effects of these different mechanisms may likely depend on cell density, flow velocity, ECM composition, and chemokine/receptor expression,[20,24] but importantly, the average result reflects shifts in cell subpopulation phenotypes.

To date, most *in vitro* studies of 3D cell invasion have used models relying on endpoint readouts that capture the average cell behavior, such as the modified 3D Boyden chamber.[22–24] However, in such assays, the typical readout—the number of cells that cross a membrane after a certain time—depends on multiple factors including the percentage of cells that are migratory, how fast they move, how persistent is their movement, and how directed they are in the direction of the membrane (*i.e.*, the flow or gradient direction). Furthermore, most migratory cell types show heterogeneous phenotypes; for example, tumor cells experience a high degree of genetic mutation upon proliferation, and dendritic cells undergo maturation at different rates, which affects their motility and chemokine receptor expression. For example, only a subpopulation of MDA-MB-231 tumor cells express CCR7, and only a subpopulation secrete its ligands CCL19 and CCL21. Therefore, in any given cell population, one may find a wide range of migrational behaviors; some may respond to flow by moving faster (but randomly), others may migrate in the flow direction through autologous chemotaxis, and still others may move in the opposite direction due to local stress gradient effects.[20] To efficiently prevent cancer cell migration and drug resistance, often resulting from cancer relapse, different populations of cells need to be targeted at the same time. When considered as a population average, as it is usually done in endpoint assays, important information useful for new treatment strategies can be lost.

Concurrently, there is increasing awareness and appreciation for the importance of the behavior of minority cell populations in cancer and immunity. Often it is small minority populations that effectively drive the important response. In cancer drug resistance, the very small percentage of cells that are not killed by chemotherapy are what later evolve to form more aggressive tumors.[27] In tumor metastasis, it is only the small fraction of cells with the phenotype required to leave the tumor and migrate to distant sites that are responsible for metastases that can kill the patient. Indeed, there is much effort right now in genetically profiling these 'minority' cell populations so that better drug regimes can be used to target different populations.[28,29] Thus, in addition to understanding the genetic differences in these minority populations, new methods are needed to evaluate their functional differences including migration behaviors.

Direct imaging of cells in 3D interstitial flow conditions has been achieved by several groups,[12,18,30–35] but quantitative insights on cell migration parameters remain scarce.[20] This is due to a multitude of factors coinciding in flow experiments. First, gels traditionally used in cell migration experiments, like collagen, Matrigel or fibrinogen, display a rather poor integrity compared to other hydrogels like agarose or gelatin.[36] Furthermore, applied fluid forces can often lead to significant gel disruption and channeling. Direct pump-driven flow (*i.e.*, fixing a flow rate as opposed to pressure gradient) can further increase flow heterogeneity and increase pressure gradients temporally and spatially within the gel. Finally, most chamber designs are difficult to use for experiments where parallel conditions are to be tested simultaneously and may be cumbersome technically for use by non-specialists.

In order to gain insight into how interstitial fluid flow directly affects cancer cells, we developed a new 3D flow chamber model, used it for live single-cell tracking of MDA-MB-231 cells, and compared different analytical approaches to reveal migration behaviors of cell subpopulations. The model possesses novel features that are well-suited for controlled, reproducible, physiologically relevant cell migration experiments including appropriate spatial dimensions and pressure-driven flow. A two-gel strategy allows maximum flexibility in flow rates and choice of cell-surrounding matrices while running four parallel assays. Interstitial flow velocities are precisely measured by fluorescence recovery after photobleaching (FRAP) with a spatial resolution of 50 μm and do not rely on the bulk estimations of fluid flow that neglect the inhomogeneous nature of the gel. The absence of clean room work makes this tool convenient for common biology labs. Furthermore, micromachining allows deeper channel heights than etched silicone wafer-based devices,[20] which is important for obtaining relevant size scales for cell migration (*i.e.*, enough so the cell is in a true 3D environment relative to its own size).

Using this new model along with different analytical approaches, we found that within a population of MDA-MB-231 cells, interstitial flow of 10 μm s^{-1} affected different cells in different ways. First, it increased the overall percentage of cells that migrate, roughly doubling the number. Second, it increased average cell speed for a majority of cells, shifting the speed histogram substantially to the right. Furthermore, while average persistence or directed migration values were similar in flow *vs.* static conditions, subpopulations of flow-directed cells were seen in histograms. Further analysis of these cells revealed that ~10% of all cells were specifically flow-responsive in the flow direction, while ~5% were flow-responsive in the negative flow direction. Together, these data underscore the heterogeneity in tumor cell migration in response to flow and demonstrate how migration data from heterogeneous cell populations can be analyzed to reveal differential effects on

different subpopulations. This type of analysis is useful for assessing how small but aggressive tumor cell subpopulations can respond to different types of inhibitors, which has ultimate application towards therapeutic strategies that target heterogeneous cell populations.

Results and discussion

Interstitial flow characterization

The flow device is shown in Fig. 1. The functional unit contained two regions for ECM gels and medium-containing regions on each side that were maintained at different pressures. PDMS pillars[30,31,37–39] were used to contain the two ECM compartments (which were injected 15 min apart) within the desired spaces due to surface tension, and maintained the borders throughout the experiment (Fig. 1A, E and F). The second gel compartment can be used for co-culture of another cell type, as has been explored by others,[37] or as a cell-free gel used to control flow rates. This feature allows the flexibility of tuning flow rates without physically altering the chamber design. In other devices, pressure-driven flow can only be tuned by the height of the pressure head itself, which can create technical difficulties in live imaging under incubator conditions. Instead, the two-gel strategy used here allows one to choose different hydrogels with desired hydraulic permeabilities[40] to limit flow without hindering cell migration within the relevant ECM encountered by the cells or increasing the pressure gradient (which was, for the experiments presented here, 7 mm H_2O). For example, the hydraulic conductivity of Matrigel varies greatly with even small changes in

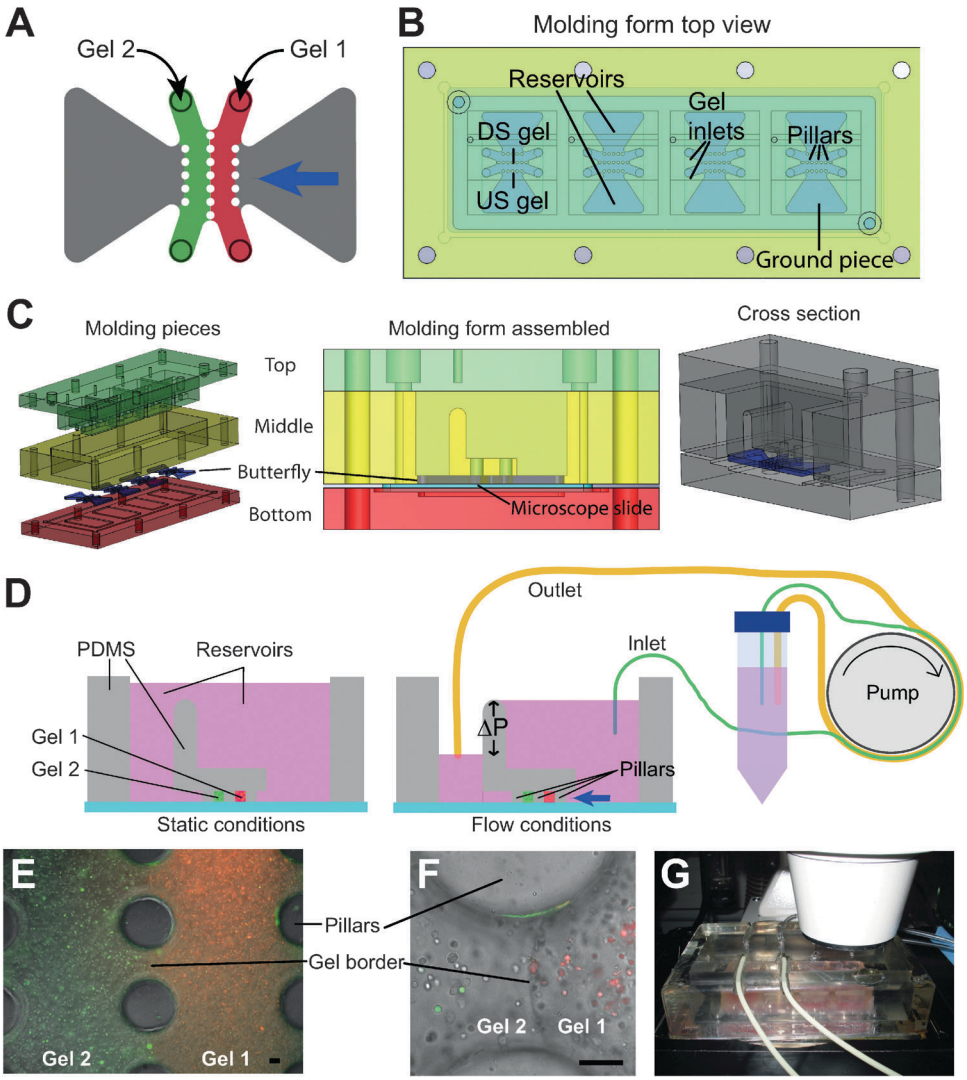

Fig. 1 Injection molding allows easy and robust set up of 4 parallel experiments on a conventional scope. (A) A single unit containing two gel compartments (upstream (US) and downstream (DS)) and medium reservoirs with different pressure heads that drive flow. (B) Top view of device shows four units on one slide, allowing parallel experimentation with a motorized microscope stage. (C) Flow chamber modules consisting of top, middle and bottom part defining the reservoirs and the butterfly-shaped ground piece creating gel channels in different perspectives as labeled. (D) Schematic of flow setup. For static conditions (left), both reservoirs are filled to the top; for flow conditions, a pressure head of 7 mm H_2O is maintained throughout the experiment with a peristaltic pump setup as shown. (E) Fluorescence microscopy image overlaid with phase of the interface between two fluorescently-labeled cell-loaded gels confined by PDMS pillars. (F) Close-up of *E* showing the gel border. (G) Chamber setup with tubing casket on an inverted microscope. Scale bars: 100 μm.

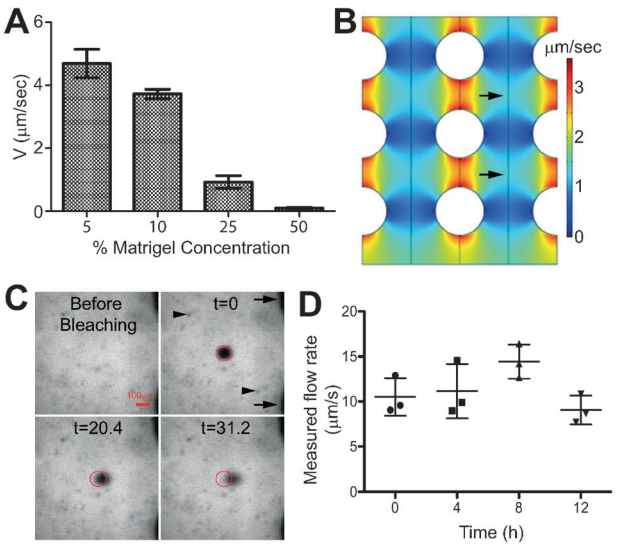

Fig. 2 Flow control and determination. (A) Flow velocity as a function of Matrigel concentration in the upstream compartment, with 1.5 mg ml^{-1} type I collagen in the downstream compartment. (B) Flow velocity profile through the matrix as predicted by Comsol modeling. Arrows indicate areas that were imaged for migration experiments; flow is from left to right. (C) Fluorescence recovery after photobleaching (FRAP) to determine local flow velocities. Red circle indicates the originally bleached area; arrowheads point to cells embedded in the gel, and arrows indicate PDMS pillars. Scale bar: 100 μm. (D) Flow velocity measured by FRAP at various times after the onset of flow, averaged from three separate locations, showing stability of the system over 12 hours.

concentration, and thus for experiments requiring very low flow velocities, flow can be diminished 50-fold by augmenting the Matrigel concentration 10-fold in the upstream channel only (Fig. 2A). This allows the possibility for a wide range of flow rates by keeping all other parameters in the cellular microenvironment constant.

A Comsol model was used to estimate flow velocity profiles around the pillars and throughout the chamber (Fig. 2B). This simulation indicated the regions where flow was most uniform (turquoise region indicated by arrows); cell migration was tracked only in these areas. FRAP was used to measure flow velocities for a fixed pressure head (Fig. 2C).

Because FRAP measures flow velocities with a temporal and spatial resolution not possible with overall averaged readouts, another advantage of our system was revealed: namely, the upstream ECM-only chamber stabilized the downstream cell-ECM compartment. Low-density collagen gels typically used in cell migration experiments are extremely soft and fragile,[41] and embedded cells can additionally degrade and deform gels locally. As revealed by FRAP, these factors can cause significant flow heterogeneity and fluid channeling (Fig. S1A, ESI‡); such flow heterogeneity was greatly diminished when Matrigel, with its higher flow resistance, was added to the chamber upstream of the cell-containing gel. By maintaining a constant pressure head over the entire length of the experiment and by measuring flow rates locally for each imaged position, we could correlate local fluid flow velocities with cellular migration behaviors. Furthermore, flow velocity was consistent for the duration of the experiment (Fig. 2D).

MDA-MB-231 cells are highly heterogeneous in their migration behavior

MDA-MB-231 human breast cancer cells were suspended in an ECM of 1.5 mg ml^{-1} type I bovine collagen and 10% Matrigel, exposed to interstitial flow velocities of 0 or 10 μm s^{-1}, and imaged over 16 h in four different chambers simultaneously (two static and two flow for each experiment) using an automated microscope stage. An interstitial velocity of 10 μm s^{-1} may be relevant in acute inflammation or in tumor microenvironments, where normal levels (0.1–1 μm s^{-1})[15] can be increased dramatically.[16,42] Furthermore, we assessed *in silico* approximations of autologous gradients that would form from such flow rates (Fig. S2, ESI‡), based on simulation parameters and methods described earlier.[25] Specifically, we estimated that at low flow rates, autologous chemokine gradients between adjacent cells may cause attraction between these cells, while this effect is reduced with increased flow velocities. This justified our use of the flow velocity tested.

After performing live cell tracking, cell tracks measured off-line (Fig. 3A) were overlaid at starting points to create polar plots; representative data are shown in Fig. 3B. Under static conditions, cell tracks remained condensed in the center of the polar plot (Fig. 3B, left), whereas in flow conditions, some of the cell tracks were notably longer (Fig. 3B, right). By measuring the tracks of each cell, we could obtain the following data for each cell as illustrated in Fig. 3C: the total distance traveled S, the net cell displacement R, and the net cell displacement in the flow direction R_f. Persistence P was calculated as R/S; average cell speed as S/time, net directed cell velocity as R_f/time, and the directed persistence P_f was R_f/R, which was also equal to $(V_f/S)/P$.

Interestingly, we observed extensive variability in migration behaviors within each experiment, reflecting a heterogeneous cell population. Only a fraction of cells migrated detectably (*i.e.*, moved at least 15 μm in 16 h), and of those, the variations in migration speed and directedness were large. Some appeared to move completely randomly, while others were clearly directed, having persistence values close to unity.

Interstitial flow increases the migrational population and speed of MDA-MB-231 cells

After calculating the individual migration parameters for each cell, we calculated averages for each experiment and then analyzed averages from four experiments (Fig. 3D). Importantly, we found that the percentage of cells considered migratory was dramatically increased by fluid flow. Furthermore, flow had a substantial effect on the average cell speed, increasing from 10 μm h^{-1} in static to 14 μm h^{-1} in flow, despite the broad heterogeneity in values. However, although many cells appeared directed in the positive or negative flow direction (*e.g.*, in Fig. 3B), there was so much variability that no significant differences were seen in directed velocity, persistence, or directed persistence (Fig. 3D).

Next, we wondered how the differences seen in % migration and average speed might be reflected in widely-used endpoint migration assays, like the modified 3D Boyden chamber with fluid flow (Fig. 3E, left).[22,24] To do this, we first carried out experiments with two different average flow velocities (limited by technical considerations), 0.4 and 4 μm s^{-1}, using the same ECM and cell density as before, and found a positive correlation

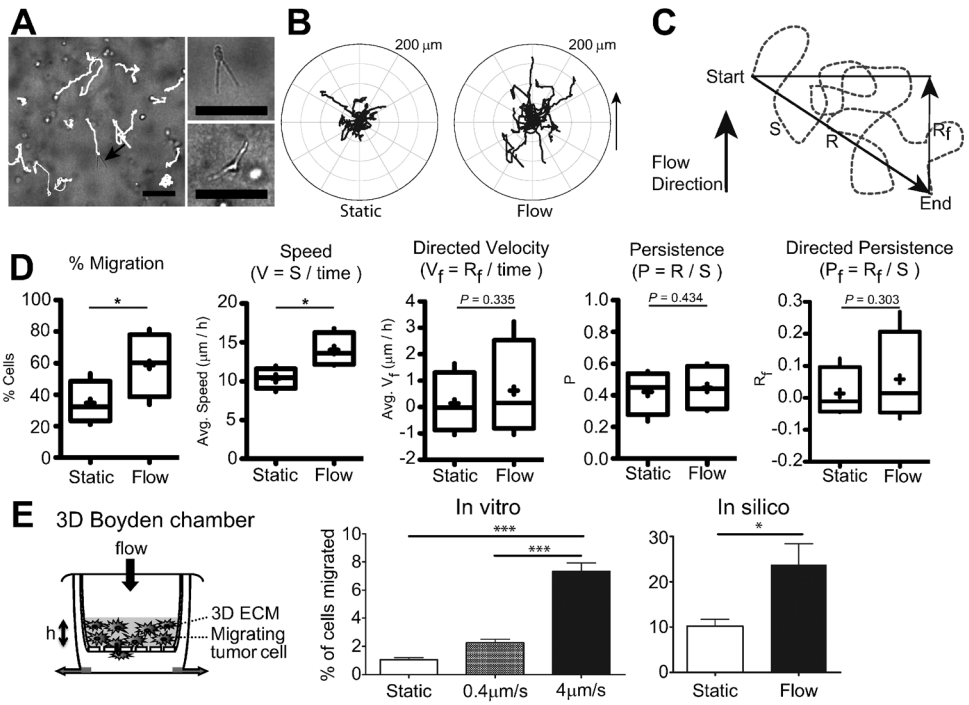

Fig. 3 Cell-averaged calculations reveal that interstitial fluid flow increases the migrational population of MDA-MB-231 cells and their average speed, but not their directed migration. (A) Left panel: Individual cells tracks (white) overlaid on phase contrast image. Arrow indicates an extended cell; scale bar, 100 μm. Inserts show two extended cells; scale bars, 50 μm. (B) Representative polar plots under static (left) and flow (right) conditions. Arrow indicates flow direction. (C) Schematic of migration parameters measured for each cell. *S* represents the total path length; *R*, the net displacement; and R_f, the net displacement in the flow direction. From these we could calculate the average cell speed (*S*/time), the directed velocity (R_f/time), the persistence (*R*/*S*), and the directed persistence ($P_f = R_f/S$). (D) Plots of population averages between four independent experiments, each with 41–169 cells tracked. (E) *In silico* and *in vitro* model of a Boyden chamber with cells migrating under static *vs.* flow conditions.

between cell transmigration and flow rate (Fig. 3E, middle). We then constructed an equivalent virtual experiment whereby the measured cell tracks, and probabilities to migrate, were applied to a randomly distributed cell population inside the 3D ECM in static *vs.* flow conditions. We calculated how many cells, given their initial position within the gel (randomly generated), migration speed, and directedness, would cross the membrane in 15 h (Fig. 3E, right). Interestingly, both in our virtual and *in vitro* experiments, interstitial flow increased cell transmigration significantly, mostly due to the combination of increased percentage of migrating cells as well as their increased overall speed under flow conditions. The differences in overall % migration seen (1–7% *in vitro* and 10–25% *in silico*) are likely due to numerous factors that were not accounted for, including edge effects in the Boyden chamber, as well as the additional barrier of cells having to transmigrate a porous membrane that was not accounted for in the virtual experiment. Thus, since endpoint assays can only measure net migration in one direction of the entire cell population, they are relatively insensitive to differences in migration parameters like random cell speed and cannot differentially examine the behavior of different cell subpopulations within a given condition, as could be seen with individual cell tracking.

Population histograms reveal cell subpopulations with directed migration parallel to flow

Because we observed more directed migration in flow *vs.* static conditions that were not reflected in the calculations of average persistence or directed persistence (Fig. 3D), we plotted histograms for the four migration parameters calculated for each cell to examine their distributions. Histograms of average cell speed (Fig. 4A) showed a clear shift in average migration speed, with both more cells moving at higher speeds as well as higher maximum speeds. The velocity in the flow direction (Fig. 4B) revealed that while similar fractions of cells were moving in the positive and negative flow directions under static *vs.* flow conditions, there was a substantially broader distribution under flow conditions, and minority subpopulations were seen migrating either with or against flow under static (Fig. 4B, arrows). The persistence histogram (Fig. 4C) also showed more cells with smaller persistence values, indicating less directed migration, although minority subpopulations with strong persistence could be seen in both static and flow conditions (Fig. 4C, arrows). Finally, the distribution of directed persistence (Fig. 5), also commonly referred to as 'chemotactic index', demonstrated a broader distribution under flow *vs.* static conditions and more cells with strong directional persistence in the flow direction.

Gating analysis allows statistical comparison of specific cell subpopulations

To determine whether the differences in migration parameters seen in directional migration could be quantified for statistical comparison, we performed gating analysis on the faster and more directed cell subpopulations. First, we plotted for each cell the average speed *vs.* their directed velocity (Fig. 5A); points that fell on a line of slope of unity in either direction would indicate cells that moved *straight* along flow

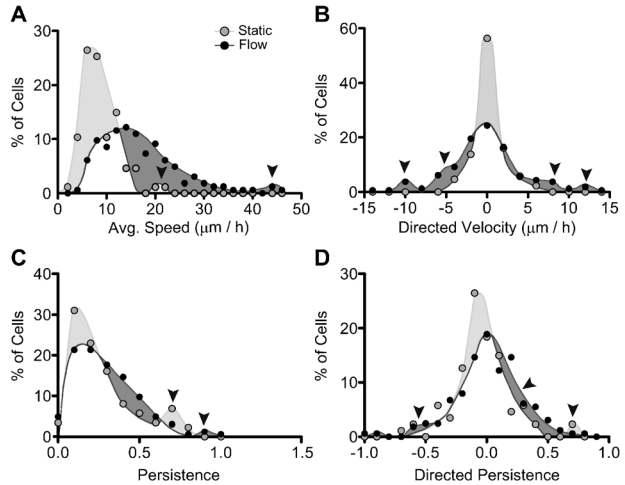

Fig. 4 Population histograms reveal subpopulations of cells with directed migration parallel to flow. All data show results from one experiment (representative of four experiments); dark shaded areas indicate where results in flow conditions (black circles) are greater than in static (open circles), and arrows show subpopulations of the data that deviate from Gaussian distribution behavior. (A) Average cell speed V (total path length divided by time), (B) directed speed V_f (net displacement in the flow direction divided by time), (C) persistence P (net displacement divided by total path length), (D) directed persistence P_f or chemotactic index (net displacement in flow direction divided by total path length). For each experiment, between 50–150 cells were analyzed for each condition.

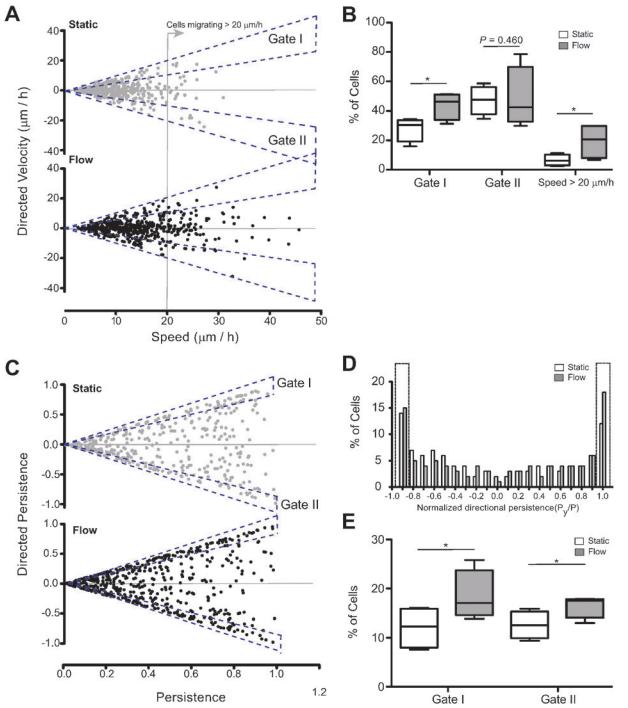

Fig. 5 Scatter plots identify the flow-responsive cell subpopulations and give further insight into their differential behavior. Scatter plots show combined data from four experiments (n = 378 and 457 cells for static and flow conditions, respectively), while box plots compares results from four sets of experiments. (A) Directed velocity V_f as a function of average cell speed, where "flow-directed" cells are gated whose directed velocity is at least 50% of the average speed in either direction. (B) Significantly more cells were defined as "flow-directed" in the flow direction under flow *vs.* static conditions. (C) Directed persistence P_f as a function of overall persistence P, showing that in flow conditions, more cells have directed persistence values that are within 90% of their overall persistence (gates I and II), indicating a significant subpopulation of flow-directed cells. (D) Histogram showing the distributions of normalized directed persistence (P_f/P) to further illustrate the clustering of cells in flow conditions near where $P_f = P$ (or $P_f/P = 1$), identifying the subpopulation of cells that respond to flow with persistence entirely along the streamlines. (E) Cell populations that moved in the flow direction (gate I) as well as those that were directed in the upstream direction (gate II) were both significantly increased in flow conditions.

streamlines—cells whose average speed was the same as their directed velocity. We then gated on cells that fell between this line and the 0.5 slope (*i.e.*, cells whose directional velocity was at least half of the average velocity); we considered these the more directionally migrating subpopulations (while conversely, cells whose V_f/V values were less than 0.5 were considered as random movers). From this, we determined that fluid flow significantly increased the fraction of cells with directed migration in the flow direction (Fig. 5B, gate I), but not in the negative flow direction (gate II). Also, we could quantify substantial increases in the fraction of cells considered "fast movers"; *i.e.*, those whose average speed was above 20 μm h^{-1} (Fig. 5B).

As another indicator of directed cell migration, we compared the persistence of each cell with its overall directed persistence (Fig. 5C). In this case, points that fall along a line of slope of unity would reflect cells whose *net displacement* was entirely directed along the flow streamlines. Here, we could see stronger effects of flow on the fraction of cells lying close to this line (Fig. 5C and D), and after gating those within 10% of this line—*i.e.*, those cells whose $P_f/P = R_f/R$ was between 0.9 and 1—we saw significantly increased directional migration in both the positive and negative flow directions of cells under flow *vs.* static conditions (Fig. 5E). In static conditions, the percentages of cells in each gate was 12 ± 4% and 13 ± 3% for gates I and II respectively, reflecting a uniform distribution and therefore random migration; this can also be seen by the histogram in Fig. 5D. In contrast, under flow conditions, 18 ± 5% of cells were strongly persistent in the flow direction, while 16 ± 2% were strongly persistent in the negative flow direction. Interestingly, by comparing the data in Fig. 5A and B and C–E, we saw a general trend that cells migrating in the negative flow direction moved with faster speeds but lower persistence, while those that migrated in the positive flow direction moved with slower speeds but more directedness.

The fact that some cells migrate towards flow while some migrate against flow reflects the heterogeneous nature of the cell population. Earlier, we showed (using endpoint assays with average cell behaviors) that some tumor cells could use autologous chemotaxis to move in the flow direction (Fig. 3E).[24] In this mechanism, cells that secrete the lymphoid homing chemokines CCL21 or CCL19 and express their receptor CCR7 could use flow to bias the secreted chemokine, causing a pericellular gradient that leads the cell through chemotactic migration mechanisms in the flow direction. However, only a small subpopulation of MDA-MB-231 cells express both CCL19 and CCR7 (Fig. S3, ESI‡), which is required for autologous chemotaxis; these fractions are

consistent with the cell fractions with flow-directed migration in the flow direction. On the other hand, a recent report suggested that MDA-MB-231 tumor cell response to flow can drive either downstream or upstream migration of individual cells, based on competing mechanisms of stress-mediated upstream migration and autologous chemotaxis-mediated mechanisms of downstream migration.[20] In that study, cell densities and flow velocities were observed to bias the relative fractions of cells moving upstream *vs.* downstream (reflected in average displacement) using different ECM compositions and flow velocities than we use here. Our general findings corroborate these conclusions and highlight the fact that only by measuring the individual cell population dynamics are we able to evaluate and compare these differential mechanisms of flow-affected cell migration.

In conclusion, we describe an experimental tool and analytical methods for analyzing the migration behavior of heterogeneous cell populations and their response to interstitial flow. We find that while interstitial flow velocities of $\sim$10 μm s^{-1} increases overall cell speed in MDA-MB-231 cells, it affects different subpopulations in different ways, causing some to migrate persistently upstream and others downstream, likely governed by different mechanisms. By evaluating behaviors of particular gated cell subpopulations, one can determine the effects of flow or blocking agents, for example, on specific cell subpopulations even if they constitute a minority of the overall population. This approach, with a focus on analyzing minority cell subpopulations that are more random or more persistent or move with faster speeds than the average cell population, is important to understand the functional differences between the invasive minority cell populations and their average, non-invasive counterparts. In turn, such analysis is critical for evaluating therapeutic interventions aimed at controlling these minority populations.

Materials and methods

Flow chamber design

The flow chamber was molded in polydimethylsiloxane (PDMS) (Sylgard 184, Dow Corning, Wiesbaden, Germany) and attached to a conventional microscope slide using silicone glue. Each of the four functional units consists of two adjoining central channels adjacent to one reservoir each. The channels were 1 mm high and constrained by 500 μm thick PDMS pillars, separated 300 μm from each other (Fig. 1A). Two different hydrogels, with or without cells embedded, can be injected in the central channels (Fig. 1E and F). After polymerization, the two reservoirs can be filled with media of different heights, creating a pressure gradient between 0–7 mm H_2O. This pressure head was maintained by a peristaltic pump throughout the experiment, siphoning medium from the lower reservoir using outlet tubes of a higher capacity whilst feeding medium using lower capacity inlet tubes (Fig. 1D). Varying hydrogel permeability allows control of interstitial flow rates across the gels. As an example, flow rates between 0.1 and 4.7 μm s^{-1} could be obtained by varying the percent of Martrigel within collagen gel mixture in the upstream channel, when maintaining a constant pressure head of 7 mm H_2O (Fig. 2A). The hydrogel in the upstream channel also plays an important role in stabilizing and distributing flow evenly across the downstream channel.

For static control conditions, chambers are filled to the top above the barrier separating the inlet and outlet regions (Fig. 1D), connecting the upstream and downstream reservoirs and thus removing any pressure gradients. Because of the parallel setup with four functional units on one conventional microscope slide (Fig. 1B and G), static and flow conditions can be directly compared within each experiment.

Master fabrication and molding

The four different parts for the injection mold (Fig. 1B and C) were micro-machined in polymethylmethacrylate on a computer numerical controlled machine (CE93; C.B. Ferrari, Modena, Italy). The structure ("butterfly") defining each functional unit with channel height, gel width and pillars (Fig. 1A) was glued with cyanoacrylate adhesive on top of a microscope slide (Fig. 1C, blue) and could be modified independently of the injection molding parts. The glass slide was held in place by the bottom part of the injection mold (Fig. 1C, red). The middle piece (Fig. 1C, yellow) defined the height of the reservoirs and was placed on top of the glass slide. The height of the reservoirs can be adjusted individually by changing only the relatively simple middle part of the injection mold. The top part of the mold was responsible for the reservoir shape and provides holes for metal poles that form the gel filling ports in the final chamber (Fig. 1C, green). This modular design provides maximal flexibility, such that key parameters like reservoir height and channel design could be modified individually.

The mold was injected with degassed PDMS, mixed according to manufacturer's recommendations and left to polymerize at 80 °C for 1 hour.

Device coating and assembly

Each device, with four functional units, was placed on a microscope slide (Menzel, Braunschweig, Germany) and edges sealed with silicon glue (Dow Corning Corp., Midland MI, USA), prior to autoclave sterilization. After oxygen plasma treatment at 200 W, 0.04 Torr for 3 minutes, a 0.01% poly-L-Lysine solution (Sigma-Aldrich Chemie GmBH, Buchs, Switzerland) was injected into the chamber and the device was incubated at room temperature for 30 minutes. Channels were flushed three times with sterile deionized (DI) water, and subsequently filled with 0.1% glutaraldehyde (Sigma-Aldrich) solution and left for 25 minutes at room temperature. Chambers were again flushed thoroughly three times with DI water and left overnight at 4 °C. Chambers were flushed and dried under vacuum for 25 minutes before gel injection.

Cell culture and cell characterization

Human MDA-MB-231 breast cancer cells were maintained in DMEM with 10% FBS and 1% Penicillin/Streptomycin (all from Gibco, Invitrogen Corp., Carlsbad, USA) until 70–80% confluence. Cells were detached with 2 mM EDTA then resuspended in L15 medium (Gibco) containing 1% Penicillin/Streptomycin. All flow experiments were conducted using L15 medium. To analyze CCR7 and CCL19 expression, MDA-MB-231s were seeded in Bovine collagen type I supplemented with 10% matrigel at 2.5×10^5 cells ml^{-1} and incubated overnight. Gels were digested with collagenase D (BD Biosciences, Franklin Lakes, NJ) and centrifuged, and cells were resuspended in 96-well plates.

After cell fixation and permeabilization with Cytofix/Cytoperm™ solution (BD Biosciences), cells were stained with anti-human PECy7-conjugated CCR7 and PE-conjugated CCL19 antibodies (1 : 400 dilution, eBioscience, San Diego, CA). Samples were acquired on CyAn™ ADP Analyzer (Beckman Coulter, Brea, CA) and analyzed with FlowJo software (Tree Star Inc., Ashland, OR).

Gel filling and device set-up

Type I Rat tail collagen (1.5 mg ml^{-1}, Becton Dickinson AG, Basel, Switzerland) was injected into the upstream gel channel of each chamber (channel 1 in Fig. 1A). Gel was polymerized for 15 min at 37 °C in a CO_2-free incubator. The second gel, consisting of 1.5 mg ml^{-1} type I Bovine collagen (Advanced BioMatrix, San Diego, CA) supplemented with 10% Matrigel and containing uniformly distributed MDA-MB-231 cells at a density of 25×10^4 cells ml^{-1}, was injected into the downstream channel (channel 2 in Fig. 1A). Chambers were turned upside down for 15 min, and right way up for a further 15 minutes, to prevent settling due to gravity, thus distributing cells evenly along the z-axis during the polymerization process. Gel inlets were sealed with heated paraffin and reservoirs were filled with media all the way to the top. Tubes were connected and fixed with the help of an additional PDMS casket (Fig. 1G). Gels were left in the incubator for another hour for complete gel polymerization before the device was transferred onto the microscope stage.

Imaging, FRAP and data analysis

For live imaging, the device was transferred onto the 37 °C incubated microscope stage. Images were taken in bright field on an inverted fluorescent microscope (Zeiss Axiovert 200 M, Carl Zeiss AG, Feldbach, Switzerland) with focus mid gel, between 400–600 μm along the z-axis, at 15 minutes intervals for 16 hours and saved for post analyses.

Flow rate across gels were measured using a fluorescent recovery after photobleaching (FRAP) technique. After cell recording was complete, FITC-dextran (2000FD, Sigma-Aldrich) was added to the medium reservoir for a final concentration of 50 μg ml^{-1}; the entire setup was subsequently transferred to a confocal microscope (Zeiss LSM 700, Carl Zeiss AG, Feldbach, Switzerland) and FRAP was carried out in the same region of interests where cell migration was imaged. A circular region of 50 μm was bleached, and images were taken every at 1 second intervals.[34]

Cell migration images were then processed off-line using ImageJ (NIH, Bethesda, MD) to track cells and an in-house Matlab script was used to determine migratory parameters. Cells were considered migratory if they moved more than 15 μm over 12 h. Any flow-induced gel drift,[3] which was always small compared to cell movements, was determined by tracking inert particles and accounted for in cell displacement measurements. For each cell track, the following measurements were made (Fig. 3C): the total pathlength S, the net distance travelled R, and the net displacement in the flow direction, R_f (equal to the vector component of R in the flow direction). Thus, for each cell we could estimate the average speed V ($=S$/time), the directed velocity V_F ($=R_f$/time), the persistence P ($=R/S$), and the directed persistence or chemotactic index P_F ($=R_f/S = V_F/V$). Positive values for V_F and P_F indicated that cells were migrating in the flow direction, while negative values indicated migration against flow. Statistics were carried out in Prism (Graphpad, La Jolla, CA, USA) for statistical analysis.

Boyden chamber transmigration experiment

Boyden chamber transmigration experiments were performed as described.[24] Briefly, 25×10^4 cells ml^{-1} MDA-MB-231 cells were dispersed in 1.5 mg ml^{-1} type I Bovine collagen supplemented with 10% Matrigel and placed into the top of an 8 mm pore size, 1 cm diameter porous culture inserts. After 30 min for polymerization, the differential level of culture medium between the top and bottom chambers was maintained at 1 cm water pressure head (for lower flow conditions) or 0 (for static conditions). For high flow conditions, a peristaltic pump was used. After 15 h at 37 °C and 5% CO_2, the number of transmigrated cells were counted using a microscope. The shape of the collagen gel (in the z-direction) within the insert was carefully measured *via* confocal microscopy to determine the meniscus (due to surface tension during polymerization) for computational studies described below (Fig. S1C, ESI‡).

Virtual Boyden chamber transmigration experiment

First, we assigned each actual cell that was tracked earlier a random starting position within the virtual 3D Boyden chamber, whose dimensions were identical to those in our *in vitro* experiment. We accounted for the meniscus in the z-direction by using the direct measurements described above; the gel volume was sectioned into 5 different radial regions, each with an average gel height and percentage of the total volume to distribute the cells appropriately (Fig. S1C, ESI‡). Then, using the actual V_f measured for each cell, we calculated the distance in the flow direction it would move over 15 h. Comparison between initial random height and migrated distance allowed us to determine how many cells would have transmigrated (*i.e.*, those whose distance migrated in the flow direction was larger than the randomly assigned distance from the membrane). A correction factor to account for the different percentages in motile cells (35% for static and 60% for flow, Fig. 3D) was applied to account for the variation in cell population motility behavior in the presence of flow.

Acknowledgements

The authors are grateful to Chiara Nembrini, Ronit Zvitov-Marabi, Hossein Madi, Simone Bottan, Brandon Dixon, Marco Pisano, and Mingming Wu for helpful advice and assistance. This study was funded by grants from the Swiss National Science Foundation (NCCR Molecular Oncology and 31-135756), the European Research Council (206653-2), and the European Framework Project 7 AngioScaff.

References

1 K. Wolf, *et al.*, Multi-step pericellular proteolysis controls the transition from individual to collective cancer cell invasion, *Nat. Cell Biol.*, 2007, **9**(8), 893–904.
2 H. D. Kim, *et al.*, Epidermal growth factor-induced enhancement of glioblastoma cell migration in 3D arises from an intrinsic increase in

speed but an extrinsic matrix- and proteolysis-dependent increase in persistence, *Mol. Biol. Cell*, 2008, **19**(10), 4249–4259.
3 Z. D. Shi, X. Y. Ji, D. E. Berardi, H. Qazi and J. M. Tarbell, Interstitial flow induces MMP-1 expression and vascular SMC migration in collagen I gels *via* an ERK1/2-dependent and c-Jun-mediated mechanism, *Am. J. Physiol.: Heart Circ. Physiol.*, 2010, **298**(1), H127–H135.
4 T. Lammermann, *et al.*, Rapid leukocyte migration by integrin-independent flowing and squeezing, *Nature*, 2008, **453**(7191), 51–55.
5 O. Ilina, G. J. Bakker, A. Vasaturo, R. M. Hofmann and P. Friedl, Two-photon laser-generated microtracks in 3D collagen lattices: principles of MMP-dependent and -independent collective cancer cell invasion, *Phys. Biol.*, 2011, **8**(1), 015010.
6 E. Cukierman and D. E. Bassi, Physico-mechanical aspects of extracellular matrix influences on tumorigenic behaviors, *Semin. Cancer Biol.*, 2010, **20**(3), 139–145.
7 S. I. Fraley, *et al.*, A distinctive role for focal adhesion proteins in three-dimensional cell motility, *Nat. Cell Biol.*, 2010, **12**(6), 598–604.
8 M. H. Zaman, *et al.*, Migration of tumor cells in 3D matrices is governed by matrix stiffness along with cell–matrix adhesion and proteolysis, *Proc. Natl. Acad. Sci. U. S. A.*, 2006, **103**(29), 10889–10894.
9 L. G. Griffith and M. A. Swartz, Capturing complex 3D tissue physiology *in vitro*, *Nat. Rev. Mol. Cell Biol.*, 2006, **7**(3), 211–224.
10 D. D. Patel, *et al.*, Chemokines have diverse abilities to form solid phase gradients, *Clin. Immunol.*, 2001, **99**(1), 43–52.
11 P. J. Wipff, D. B. Rifkin, J. J. Meister and B. Hinz, Myofibroblast contraction activates latent TGF-beta1 from the extracellular matrix, *J. Cell Biol.*, 2007, **179**(6), 1311–1323.
12 C. L. Helm, M. E. Fleury, A. H. Zisch, F. Boschetti and M. A. Swartz, Synergy between interstitial flow and VEGF directs capillary morphogenesis *in vitro* through a gradient amplification mechanism, *Proc. Natl. Acad. Sci. U. S. A.*, 2005, **102**(44), 15779–15784.
13 D. Seliktar, A. H. Zisch, M. P. Lutolf, J. L. Wrana and J. A. Hubbell, MMP-2 sensitive, VEGF-bearing bioactive hydrogels for promotion of vascular healing, *J. Biomed. Mater. Res.*, 2004, **68**(4), 704–716.
14 A. C. Shieh and M. A. Swartz, Regulation of tumor invasion by interstitial fluid flow, *Phys. Biol.*, 2011, **8**(1), 1–8.
15 S. R. Chary and R. K. Jain, Direct measurement of interstitial convection and diffusion of albumin in normal and neoplastic tissues by fluorescence photobleaching, *Proc. Natl. Acad. Sci. U. S. A.*, 1989, **86**(14), 5385–5389.
16 D. O. Bates, N. J. Hillman, B. Williams, C. R. Neal and T. M. Pocock, Regulation of microvascular permeability by vascular endothelial growth factors, *J. Anat.*, 2002, **200**(6), 581–597.
17 H. Dafni, T. Israely, Z. M. Bhujwalla, L. E. Benjamin and M. Neeman, Overexpression of vascular endothelial growth factor 165 drives peritumor interstitial convection and induces lymphatic drain: magnetic resonance imaging, confocal microscopy, and histological tracking of triple-labeled albumin, *Cancer Res.*, 2002, **62**(22), 6731–6739.
18 C. P. Ng, B. Hinz and M. A. Swartz, Interstitial fluid flow induces myofibroblast differentiation and collagen alignment *in vitro*, *J. Cell Sci.*, 2005, **118**(Pt 20), 4731–4739.
19 K. R. Levental, *et al.*, Matrix crosslinking forces tumor progression by enhancing integrin signaling, *Cell*, 2009, **139**(5), 891–906.
20 W. J. Polacheck, J. L. Charest and R. D. Kamm, Interstitial flow influences direction of tumor cell migration through competing mechanisms, *Proc. Natl. Acad. Sci. U. S. A.*, 2011, **108**(27), 11115–11120.
21 J. A. Pedersen, S. Lichter and M. A. Swartz, Cells in 3D matrices under interstitial flow: effects of extracellular matrix alignment on cell shear stress and drag forces, *J. Biomech.*, 2010, **43**(5), 900–905.
22 H. Qazi, Z. D. Shi and J. M. Tarbell, Fluid Shear Stress Regulates the Invasive Potential of Glioma Cells *via* Modulation of Migratory Activity and Matrix Metalloproteinase Expression, *PLoS One*, 2011, **6**(5), e20348.
23 A. Shieh, H. Rozansky, B. Hinz and M. A. Swartz, Tumor cell invasion is promoted by interstitial flow-induced matrix priming by stromal fibroblasts, *Cancer Res.*, 2011, **71**(3), 790–800.
24 J. D. Shields, *et al.*, Autologous chemotaxis as a mechanism of tumor cell homing to lymphatics *via* interstitial flow and autocrine CCR7 signaling, *Cancer Cell*, 2007, **11**(6), 526–538.
25 M. E. Fleury, K. C. Boardman and M. A. Swartz, Autologous morphogen gradients by subtle interstitial flow and matrix interactions, *Biophys. J.*, 2006, **91**(1), 113–121.
26 G. J. Randolph, V. Angeli and M. A. Swartz, Dendritic-cell trafficking to lymph nodes through lymphatic vessels, *Nat. Rev. Immunol.*, 2005, **5**(8), 617–628.
27 D. Hanahan and R. A. Weinberg, Hallmarks of Cancer: The Next Generation, *Cell*, 2011, **144**(5), 646–674.
28 M. T. Agullo-Ortuno, F. Lopez-Rios and L. Paz-Ares, Lung Cancer Genomic Signatures, *J. Thoracic Oncol.*, 2010, **5**(10), 1673–1691.
29 C. Coghlin and G. I. Murray, Current and emerging concepts in tumour metastasis, *J. Pathol.*, 2010, **222**(1), 1–15.
30 C. P. Ng and S. H. Pun, A perfusable 3D cell–matrix tissue culture chamber for *in situ* evaluation of nanoparticle vehicle penetration and transport, *Biotechnol. Bioeng.*, 2008, **99**(6), 1490–1501.
31 V. Vickerman, J. Blundo, S. Chung and R. Kamm, Design, fabrication and implementation of a novel multi-parameter control microfluidic platform for three-dimensional cell culture and real-time imaging, *Lab Chip*, 2008, **8**(9), 1468–1477.
32 C. P. Ng, C. L. Helm and M. A. Swartz, Interstitial flow differentially stimulates blood and lymphatic endothelial cell morphogenesis *in vitro*, *Microvasc. Res.*, 2004, **68**(3), 258–264.
33 C. P. Ng and M. A. Swartz, Fibroblast alignment under interstitial fluid flow using a novel 3-D tissue culture model, *Am. J. Physiol. Heart Circ. Physiol.*, 2003, **284**(5), H1771–H1777.
34 C. Bonvin, J. Overney, A. C. Shieh, J. B. Dixon and M. A. Swartz, A multichamber fluidic device for 3D cultures under interstitial flow with live imaging: development, characterization, and applications, *Biotechnol. Bioeng.*, 2010, **105**(5), 982–991.
35 R. Hernandez Vera, *et al.*, Interstitial fluid flow intensity modulates endothelial sprouting in restricted Src-activated cell clusters during capillary morphogenesis, *Tissue Eng. A*, 2009, **15**(1), 175–185.
36 J. A. Pedersen and M. A. Swartz, Mechanobiology in the third dimension, *Ann. Biomed. Eng.*, 2005, **33**(11), 1469–1490.
37 C. P. Huang, *et al.*, Engineering microscale cellular niches for three-dimensional multicellular co-cultures, *Lab Chip*, 2009, **9**(12), 1740–1748.
38 R. Sudo, *et al.*, Transport-mediated angiogenesis in 3D epithelial coculture, *FASEB J.*, 2009, **23**(7), 2155–2164.
39 S. Chung, *et al.*, Cell migration into scaffolds under co-culture conditions in a microfluidic platform, *Lab Chip*, 2009, **9**(2), 269–275.
40 M. A. Swartz and M. E. Fleury, Interstitial flow and its effects in soft tissues, *Annu. Rev. Biomed. Eng.*, 2007, **9**, 229–256.
41 K. Wolf, *et al.*, Collagen-based cell migration models *in vitro* and *in vivo*, *Semin. Cell Dev. Biol.*, 2009, **20**(8), 931–941.
42 A. Ruddell, *et al.*, Dynamic contrast-enhancedmagnetic resonance imaging of tumor-induced lymph flow, *Neoplasia*, 2008, **10**(7), 706–713, 701 p following 713.